The Thesis Committee for Sarah Catherine Mason
Certifies that this is the approved version of the following thesis:

Femtosecond time-domain thermoreflectance measurements of cross-plane thermal conductivity of GaAs/AlAs superlattices

APPROVED BY
SUPERVISING COMMITTEE:

Supervisor:

Yaguo Wang

Li Shi

Femtosecond time-domain thermoreflectance measurements of cross-plane thermal conductivity of GaAs/AlAs superlattices

by

Sarah Catherine Mason, B.S.M.E

Thesis

Presented to the Faculty of the Graduate School of

The University of Texas at Austin

in Partial Fulfillment

of the Requirements

for the Degree of

Master of Science in Engineering

The University of Texas at Austin

May 2017

Acknowledgements

I would first like to thank my parents for their support and encouragement throughout my life. I would also like to thank my husband for encouraging me to attend graduate school, even though we spent most of our engagement in separate cities. To my brother, thank you for helping me with my homework during all the years I was in school.

I could not have done all the work in this thesis without the help of the other members of our research group. Feng, thank you for helping me test all the samples and teaching me about the experimental setups. Jihoon, thank you for helping me understand the thermal model and troubleshooting all my Matlab problems. Ke and Xianghai, thank you for the many discussions about the physics involved in this work.

I would like to thank The University of Texas at Austin Graduate School and Cockrell School of Engineering for their financial support.

Finally, I would like to thank my supervisor, Dr. Wang. I would not have been able to come back to UT to get my Masters with your help. Thank you for guiding and encouraging me through these past two years.

Abstract

Femtosecond time-domain thermoreflectance measurements of cross-plane thermal conductivity of GaAs/AlAs superlattices

Sarah Catherine Mason, M.S.E

The University of Texas at Austin, 2017

Supervisor: Yaguo Wang

Nanostructuring is a proven method to reduce the thermal conductivity and increase the thermoelectric figure of merit of semiconductor materials for applications such as solid-state refrigeration. Accurate measurement of the thermal properties of nanostructured materials is necessary to utilize them properly. One technique to measure the cross-plane thermal conductivity of these materials is time-domain thermoreflectance (TDTR). In TDTR, the sample is coated with a thin metal layer which is heated by a laser pulse. As the metal layer cools by heat conduction into the sample, the change in optical reflectivity is detected by a probe laser. For temperature changes of a few kelvin, the change in probe reflectivity is directly proportional to the change in temperature of the metal. By comparing the experimental measurements to a simulated one-dimensional conduction heat flow analysis, the thermal conductivity of the sample and the thermal boundary resistance between the metal and the sample can be determined. In this thesis, we use TDTR to measure the cross-plane thermal conductivity of seven GaAs/AlAs superlattices with period thickness ranging from 2 nm to 41 nm. We compare the results

from two TDTR setups, one uses a Ti:sapphire oscillator system with a repetition rate of 76 MHz and the other uses an amplifier system with a repetition of 5 kHz. Most of the thermal conductivity values from the amplifier measurements are consistent with the literature values. However, most of the thermal conductivity values from the oscillator measurements are larger than the literature values. The discrepancy is likely due to pulse accumulation. A sensitivity analysis of the thermal model shows a time delay of at least 2.5 ns should be used to minimize the uncertainty of the thermal boundary resistance measurement. Generally, increasing the time delay will further reduce the uncertainty of the thermal conductivity, but the diffusion length within the superlattice at the maximum time delay also has to be considered. The minimum superlattice thickness that can be measured within the 2.5 ns time delay without substrate interaction is about 120 nm for material with a diffusivity of 6×10^{-6} m^2/s.

Table of Contents

List of Tables

List of Figures

Chapter 1: Introduction

1.1: MOTIVATION

The devices and features in microelectronics continue to get smaller and more powerful. However, thermal management is one of the factors limiting the advancement of this technology. Thermal conductivity is a measure of a material's ability to conduct heat. It depends on temperature, and it can be anisotropic in some materials (cross-plane and in-plane). High thermal conductivity is required for systems, such as computer processors, where heat generation needs to be effectively removed. In applications such as solid-state refrigeration and thermal barriers, where heat flow needs to be minimized, materials with very low thermal conductivity are needed [1].

The thermoelectric figure of merit, $ZT=S^2\sigma T/\kappa$, where S is the Seebeck coefficient, σ is the electrical conductivity, T is the absolute temperature, and κ is the thermal conductivity, is a measure of the efficiency of thermoelectric energy conversion. Reduction of the thermal conductivity through nanostructuring has been shown effective to increase the thermoelectric figure of merit [2, 3]. Nanostructuring materials allows for engineering of properties that are not found in their bulk constituent materials. For example, a superlattice made of GaAs and AlAs with a superlattice period smaller than approximately 10nm has been shown to have a thermal conductivity below the alloy limit, and the thermal conductivity can be reduced by a factor of 10 at room temperature compared to bulk [4].

A superlattice is a film made of alternating layers of two materials. In nonmetallic systems, such as GaAs/AlAs, heat is transported mainly by phonons. The kinetic model for thermal conductivity defines $\kappa = C_v v^2 \tau_{ph}$, where C_v is the phonon heat capacity, v is the average phonon velocity component along the transport direction, and τ_{ph} is the

average phonon lifetime. When the phonon mean free paths are larger than or comparable to the superlattice period, modification of the phonon dispersion in superlattices can potentially play a role if the interface roughness is much smaller than the wavelength of the phonon mode. Zone folding and polarization gaps in the modified phonon dispersion can result in reduced phonon group velocities and increased scattering, both of which contribute to the reduction of the thermal conductivity [5].

1.2: OUTLINE

In this thesis, the cross-plane thermal conductivities of several GaAs/AlAs superlattices are measured using time-domain thermoreflectance with a high repetition rate pulsed laser and a low-repetition rate laser. Chapter 2 gives a brief overview of three techniques widely used for cross-plane thermal conductivity measurements in thin films: 3ω, frequency-domain thermoreflectance (FDTR), and time-domain thermoreflectance (TDTR). Chapter 3 gives a more detailed explanation of the technique used in this work, TDTR. It includes information about the evolution of the TDTR technique and important contributions to the analysis of the data. Chapter 3 also includes descriptions of the two experimental apparatus and the thermal analysis used to obtain the thermal properties for the GaAs/AlAs samples. In chapter 4, the structure of the samples that were tested are described and the experimental data is presented and discussed along with a sensitivity analysis. Chapter 5 includes recommendations for improving and expanding the work done in this thesis. Finally, chapter 5 also summarizes the conclusions drawn from the analysis and results presented.

Chapter 2: Overview of Thermal Conductivity Measurement Techniques

Accurate measurement of the thermal properties of superlattices is needed to properly utilize the unique advantages they offer. In addition to the thermal conductivity, the thermal boundary resistance is also critically important to understand the heat flow. The thermal boundary resistance, R_{th}, with units of m^2K/W, is the ratio between temperature drop and heat flux across the interface where two components meet. It depends on the deposition method and the properties of the materials. Three techniques are widely used to measure the cross-plane thermal conductivity of superlattices and thin films: 3ω [6, 7], frequency-domain thermoreflectance (FDTR) [8], and time-domain thermoreflectance (TDTR) [9, 10, 4].

2.1: 3ω METHOD

The 3ω method was introduced by Cahill in 1987 [11]. In the 3ω technique, a narrow metal line, which acts as both a heater and a thermometer, is patterned on the sample film using microfabrication. An electrical current of frequency ω applied to the metal line heats the sample with a frequency of 2ω. The voltage oscillation in the metal line resulting from the 2ω temperature oscillation (resistance oscillation) and the ω current oscillation has a frequency of 3ω. The amplitude of the voltage oscillation is measured, and the thermal conductivity can easily be determined from this measurement [11]. The 3ω technique has a lower cost and a much simpler setup and data analysis than the thermoreflectance methods. The minimum film thickness is defined by the thermal penetration depth, $d = \sqrt{D/(\pi f)}$, where D is the thermal diffusivity and f is the frequency of the oscillation. The frequency in 3ω measurements ranges from 5 Hz to 200 KHz which sets a minimum film thickness on the order of microns [12]. Because of this

large spatial resolution, the 3ω cannot determine the thermal boundary resistance at the interfaces of the film [13]. Additionally, the metal line has to be electrically isolated from the film, so a thin layer of dielectric is necessary if the film is electrically conductive. This dielectric layer creates another thermal resistance which can lower the technique's sensitivity and accuracy. The overall uncertainty of the film's thermal conductivity measurement is approximately 25% [12].

2.2: FREQUENCY-DOMAIN THERMOREFLECTANCE

Frequency-domain thermoreflectance and time-domain thermoreflectance are both non-contact, optical techniques for measuring thermal conductivity. In both methods, a pump and a probe beam are concentrically focused on a thin metal transducer layer that has been deposited on top of the sample. The metal layer absorbs the pump light, creating an increase in temperature. As the transducer layer cools by conduction into the sample layer, the optical reflectivity of the transducer layer changes proportionally to the temperature change. The change in reflectivity is detected by the probe beam and measured by a lock-in amplifier, creating a cooling curve. The experimental results are then compared to a simulation of the heat flow where the thermal conductivity of the sample and the thermal boundary resistance between the transducer and the sample are adjusted until the model fits the experimental results [4]. The metal transducer lay does add an additional step to the sample preparation process, but it is minimal compared to the microfabrication requires for the 3ω technique.

The difference between FDTR and TDTR is that in FDTR, the reflectance change is measured as a function of the modulation frequency at a fixed time delay between the pump and probe beams. This eliminates errors associated with motion of the delay stage, divergence of the beams, and changes in the overlap of the beams [14]. FDTR can

measure thinner samples than TDTR because a higher modulation frequency is usually used [14], but the uncertainty of the thermal conductivity measurement, which is primarily due to the accuracy of the transducer thickness and the laser spot radii, is generally higher for FDTR measurements compared to TDTR measurements for thinner films [15].

2.3: TIME-DOMAIN THERMOREFLECTANCE

In TDTR the reflectance change of the transducer is measured as a function of delay time between the pump and probe beams. The time delay can range from 100 ps [16] to several microseconds [17]. Femtosecond-TDTR (fs-TDTR) uses a mode-locked laser with a pulse duration of less than 1 picosecond. This requires more complex, expensive equipment than FDTR which uses a continuous-wave (cw) laser [8]. However, fs-TDTR is more sensitive to the interface resistance between the transducer and the sample than FDTR [15]. Depending on the diffusivity of the thin film and the modulation frequency, the minimum film thickness for fs-TDTR is approximately 60nm. The overall uncertainty of the thermal conductivity measurement with TDTR, which is limited by the uncertainty of the transducer film thickness, is about 7% [12]. A more detailed discussion of the fs-TDTR experimental setup and data analysis is included in the next section. TDTR using Q-switched nanosecond lasers is called nanosecond-TDTR (ns-TDTR) [18] or nanosecond transient thermoreflectance (TTR) [17]. The setup is much simpler compared to fs-TDTR because there is no delay stage, but, like the 3ω method, the large time scale means the measurable minimum film thickness is larger and the thermal conductivity of the film cannot be separated from the thermal boundary resistances at its interfaces [13]. The biggest advantages of FDTR and fs-TDTR over 3ω are the decreased

minimum film thickness, improved uncertainty, and the ability to isolate the thermal boundary resistance from the thermal conductivity of the film.

Chapter 3: Details of Time-Domain Thermoreflectance

Throughout the rest of this thesis, for simplification, TDTR will refer to fs-TDTR. In this section, the development and improvement over time of the TDTR method for measuring the cross-plane thermal conductivity of thin films will be discussed. The experimental apparatus and thermal models used to acquire the data and thermal properties shown in chapter 4 are also detailed here.

3.3: Chronology of TDTR

In 1986, Paddock and Eesley [19] were the first to use picosecond thermoreflectance to measure the thermal diffusivity of nanometer-scale thin films. The other techniques available at the time required knowing the thermal properties of the substrate, but by using a small time delay (<200 ps), they were able to measure the diffusivity of the 100 nm thick metal film independent of the substrate. They numerically solved the one-dimensional conduction equation while treating the thermal diffusivity of the film as a free parameter until the difference between the experimental curve and the model was minimized [16].

In 1996, Capinski and Maris [20] were among the first to report the thermal conductivity of short-period superlattices (SL). They conducted a fairly complete study of the thermal conductivity of GaAs/AlAs superlattice samples with periods ranging from two monolayers (1 monolayer GaAs and 1 monolayer of AlAs) to 80 monolayers (40 monolayers GaAs and 40 monolayers of AlAs). To resolve the thermal conductivity of the SL, Capinski and Maris et al. used a maximum time delay of 7.5 ns [4]. The large time delay can introduce significant errors due to changes in the overlap of the pump and probe beams making accurate measurements difficult. To solve this issue, they added an

optical fiber to their apparatus after the mechanical delay stage. The optical fiber allows for a constant beam profile regardless of the position of the mechanical delay stage [21].

Capinski and Maris et al. [4] were also the first to include the effects of pulse accumulation in the analysis of the signal recorded by the lock-in amplifier. The pump and probe beams were produced by an oscillator system with a 76 MHz repetition rate which means a heating pulse arrives at the sample about every 13 ns. The simple one-dimensional conduction equation used by Paddock and Eesley [16] assumed the thermal response to each pump pulse fell to a negligible value before the next pulse arrived. However, in most thermal conductivity measurements with high repetition rate systems, that assumption is incorrect [22], so the contributions to the signal from the previous pulses must be considered. Capinski and Maris solved the one-dimensional conduction equation numerically with assumed values for the SL thermal conductivity and thermal boundary resistance to calculate the change in temperature of the metal transducer film. Then, they used that change in temperature due to a single pump pulse to calculate the simulated lock-in signal that accounts for the pulse accumulation. Similarly to Paddock and Eesley, Capinski and Maris et al. changed the assumed values for thermal conductivity and the thermal resistance until the error between the model and the experimental data was minimized [4].

Cahill developed the 3ω method [11], but he and his group began to contribute heavily to the development [1, 13, 23] and applications [24, 25, 26, 27] of TDTR in the early 2000s. Capinski and Maris [21] used an optical fiber to correct for changes in the overlap of the beams and defocusing of the pump, but Cahill [13] took advantage of the out-of-phase signal from the lock-in amplifier for a much simpler fix. Since the in-phase (V_{IN}) and out-of-phase (V_{OUT}) signals are both affected by changes in the overlap of the beams and defocusing of the pump, using the ratio of the in-phase signal to out-of-phase

signal effectively cancels out the errors. Lyeo and Cahill [28] also noted that V_{OUT} is more sensitive to the thermal boundary conductance than V_{IN}, so using V_{IN}/ V_{OUT} will give a better measurement of the conductance than only using V_{IN}. For a more quantitative understanding of the sensitivity of the model to various parameters, the sensitivity can be calculated as the logarithmic derivative of the signal with respect to the logarithmic derivative of the parameter of interest [24].

While previous works analyzed the heat flow in the time domain, Cahill [23] instead analyzed the heat flow of TDTR in the frequency domain. Since the sample is heated by a modulated periodic point source, similar to the 3ω method, the thermal response has a frequency component that can be used to calculate the in-phase and out-of-phase signals from the lock-in amplifier. This allows the lock-in signals to be calculated analytically, rather than using a numerical method such as finite difference, so the problem of convergence caused by choice of spatial and temporal time steps is no longer an issue.

3.2: EXPERIMENTAL APPARATUS

In this thesis, two different experimental setups were used to measure TDTR data. One setup uses an oscillator system with a high repetition rate to produce the pump and probe beams. The other setup uses an amplifier system with a low repetition rate to produce the pump and probe beams. The two experimental apparatus are described and compared in this section.

3.2.1: Oscillator

A schematic of the oscillator apparatus used in this thesis is depicted in Figure 1. The light pulses are produced by a Ti:sapphire laser at a repetition rate of 76 MHz, a pulse duration of 30 fs, and a wavelength of 800 nm. The beam is split into a pump beam,

which is modulated at a frequency of about 2 kHz by a mechanical chopper and focused to a spot diameter of about 70 um on the sample, and a probe beam, which is reflected off of a retroreflector on a mechanical delay stage and then focused to a spot diameter of about 30 um on the sample. The energies of each pump and probe pulse are approximately 0.3 nJ and 0.03 nJ, respectively. The change in probe intensity caused by the cooling of the sample is extracted by a lock-amplifier which uses the pump modulation frequency as a reference to improve the signal-to-noise ratio. The CCD is used to ensure the overlap of the pump and probe.

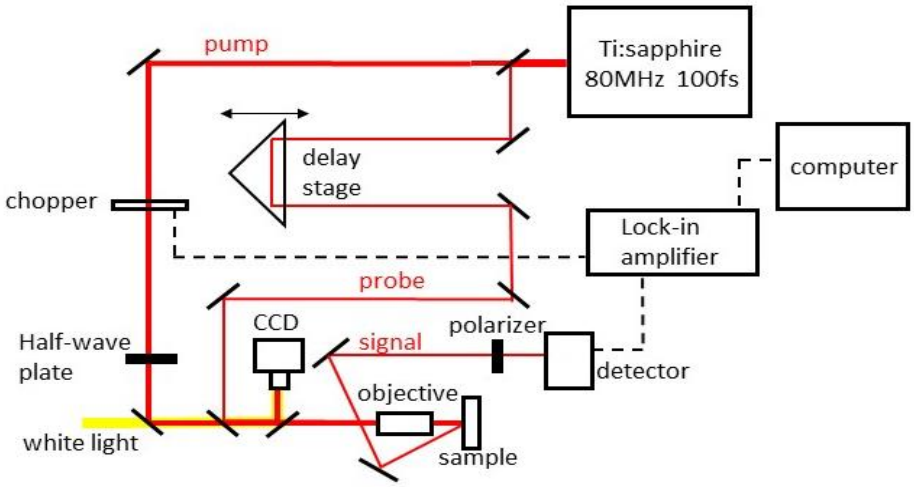

Figure 1: Schematic of TDTR experimental apparatus with Ti:sapphire oscillator producing light pulses at a repetition rate of 76 MHz, pulse duration of 30 fs, and wavelength of 800 nm.

Because of the low modulation frequency of the mechanical chopper, compared to the higher (>1 MHz) modulation frequencies that can be achieved with acousto- and electro-optic modulators, the out-of-phase signal does not change, so only the in-phase signal is used in analysis. The mechanical chopper was used due to constraints of available equipment. In Cahill's apparatus [13], the pump beam goes though the delay

stage, rather than the probe beam. This method requires careful monitoring of the pump intensity profile at long time delays to ensure consistent heating. Cahill also uses the same diameter for the pump and probe spots [23] which creates additional concerns about maintaining the pump-probe overlap. The probe spot diameter in our apparatus is about one-half the size of the pump spot, so even if the probe is misaligned slightly at long time delays, it stays within the uniformly heated area (near the center of the pump).

3.2.2: Amplifier

In the amplifier apparatus, illustrated in Figure 2, the light pulses are produced by a Ti:sapphire amplifier at a repetition rate of 5 kHz, a pulse duration of 35 fs, and a wavelength of 800 nm. The beam is split into a pump beam and a probe beam. The pump beam is frequency doubled by a BBO crystal, modulated at a frequency of 585 Hz by a mechanical chopper, and focused to a spot diameter of about 245 um on the sample. The probe beam is reflected off of a retroreflector on a mechanical delay stage and then focused to a spot diameter of about 60 um on the sample. The energies of each pump and probe pulse are approximately 140 nJ and 0.136 nJ, respectively. The change in probe intensity caused by the cooling of the sample is extracted by a pre-amplifier that is connected to a lock-in amplifier which uses the pump modulation frequency as a reference to improve the signal-to-noise ratio. The CCD is used to ensure the overlap of the pump and probe. Because of the low modulation frequency of the mechanical chopper, only the in-phase signal is used in analysis. The divergence of the probe is less than 5% over the time delay used, so the error that may be associated with only using V_{IN}, rather than V_{IN}/V_{OUT} is negligible.

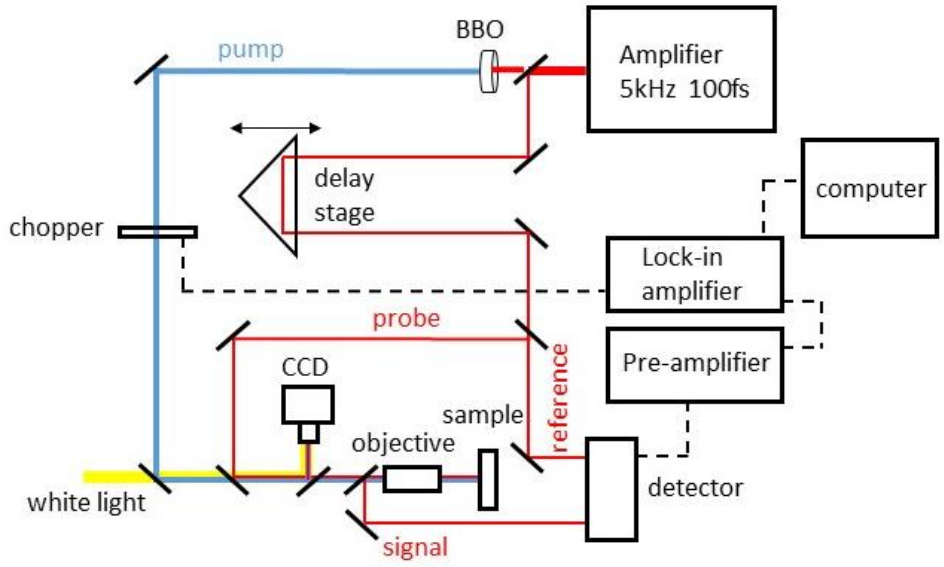

Figure 2: Schematic of TDTR experimental apparatus with an amplifier producing light pulses at a repetition rate of 5 kHz, pulse duration of 35 fs, and wavelength of 800 nm.

3.2.3: Comparison of apparatus

The biggest difference between the oscillator and amplifier setups is the production of the light pulses. The majority [4, 13, 29, 30] of TDTR experiments use an oscillator system because it is simpler and less expensive than the amplifier system. It may also have a better signal-to-noise ratio if pump modulation and lock-in detection is at a high frequency [22], but the low-repetition rate of the amplifier eliminates the errors associated with pulse accumulation and makes the analysis of the signal much simpler. A pump pulse arrives at the sample every 13.1 ns in the oscillator system and every 0.2 ms in the amplifier system. This means that, in the amplifier apparatus, the sample's response to the pump pulse is much more likely to have fallen to a negligible value before the next pump pulse, so the effects of the previous pulses do not need to be included in the analysis.

Another difference between the two experimental setups is the use of the BBO crystal to double the frequency of the pump beam in the amplifier apparatus. Changing the wavelength of the pump makes it easier to separate the probe signal from unwanted scattered pump light into the detector. In the oscillator apparatus, using a polarizer to isolate the probe signal makes the optics slightly more complicated. It is possible to implement the two-color arrangement in the oscillator setup, but the BBO crystal is more effective at the higher pulse energies that can be achieved with the amplifier. Additionally, the oscillator and amplifier systems were used for experimental techniques other than TDTR, so the setups were designed to reduce changes to the setups between experiments.

3.3: MODEL FOR ANALYSIS OF HEAT FLOW

One-dimensional conduction in the cross-plane direction is used to describe the heat flow through the three-layer samples in TDTR. Paddock and Eesley [16] assumed one-dimensional conduction in their analysis because the pump diameter was much larger than the thermal penetration depth. Capinski and Maris et al. [4] calculated the change in reflectivity that would occur if the transducer layer could only cool in the radial direction. The change in reflectivity due to radial heat diffusion was negligible within the time delay of the experiment, so one-dimensional was a valid approximation. Norris et al. [31] assumed one-dimensional heat flow in their work when the pump spot was much larger than the thickness of the film of interest. None of these conditions to assume one-dimensional heat flow seem complete by themselves, so we will check whether each one is valid for our experiments. They all depend on the size of the heated area, but the first depends on the temporal heating event, the second depends on the diffusivity of the material, and the third depends on the thickness of the film.

To test whether the first condition applies to our experiment, we can use the diffusion length $L = \sqrt{D\tau}$ to define the thermal penetration depth in the metal layer and the SL. First, to determine if one-dimensional heat flow is valid in the metal transducer layer, we calculate the diffusion length using the thermal diffusivity of the metal, D=8x10^{-5} m^2/s for aluminum, and the laser pulse duration at the sample, about 30 fs, for τ. This gives a thermal penetration depth of less than 2 nm which is far smaller than the diameter of the pump. To determine if one-dimensional heat flow is valid in the SL, we calculate the diffusion length using the diffusivity of the SL, D<2.8x10^{-5} m^2/s for the samples tested, and the longest time delay, 2.5 ns, for τ. This gives a thermal penetration depth of less than 300 nm, which is still significantly smaller than the pump diameter. For the next condition, we are able to verify that the change of reflectivity due to radial heat diffusion is smaller than what Capinski and Maris calculated because our pump spot is at least seven times larger than theirs. For the third condition, our pump spot in both experimental setups is much larger than the thicknesses of the superlattice films. Our experiments meet all three conditions stated above; thus the assumption of one-dimensional heat flow in the cross-plane direction should be valid.

Our analysis is done in the time domain and the heat conduction equation is solved using the finite difference method. The analysis starts with describing the one-dimensional conduction in the cross-plane direction (z-direction) in the metal transducer layer heated by a single pump pulse defined as:

$$C_M \frac{\partial T_M(z,t)}{\partial t} = \kappa_M \frac{\partial^2 T_M(z,t)}{\partial z^2} + I(1-R)\alpha e^{-\alpha z} e^{-\left(\frac{t}{\tau}\right)^2} \quad (1)$$

where C_M is the heat capacity of the metal, $T_M(z,t)$ is the temperature profile in the metal at time t and distance z from the surface, κ_M is the thermal conductivity of the metal, I is the laser intensity, R is the reflectivity of the metal, α is the absorption coefficient of the metal, and τ is the laser pulse duration. Because we solve for the

temperature distribution in the metal transducer layer, this analysis can be used for a two-layer (thin metal film and substrate) structure or a three-layer (transducer, superlattice, and substrate) structure. For a two-layer structure, the material properties for the substrate are used in both the second and third layers and the thermal boundary resistance between the second and third layers is set to 0. In the analysis by Capinski and Maris et al. [4], the change in temperature, rather than the temperature profile, in the transducer layer caused by the heating pulse was calculated and used as an initial condition. This may reduce calculation time, but it also reduces the flexibility of the model.

The heat flow at the interface between the metal transducer layer and the superlattice layer is given by:

$$C_M d_M \frac{\partial T_M(z=d_M,t)}{\partial t} = -\frac{[T_M(z=d_M,t)-T_{SL}(z=d_M,t)]}{R_{th,M-SL}} \quad (2)$$

where d_M is the thickness of the metal transducer layer, $T_{SL}(z = d_M, t)$ is the temperature at the top surface of the superlattice, and $R_{th,M-SL}$ is the thermal boundary resistance between the metal film and the superlattice. The heat flow within the superlattice is given by:

$$C_{SL} \frac{\partial T_{SL}(z,t)}{\partial t} = \kappa_{SL} \frac{\partial^2 T_{SL}(z,t)}{\partial z^2} \quad (3)$$

where C_{SL} is the heat capacity of the superlattice, $T_{SL}(z,t)$ is the temperature profile in the superlattice at time t and distance z from the metal surface, and κ_{SL} is the thermal conductivity of the superlattice. The heat flow at the interface between superlattice and substrate is given by:

$$C_{SL} d_{SL} \frac{\partial T_{SL}(z=d_M+d_{SL},t)}{\partial t} = -\frac{[T_{SL}(z=d_M+d_{SL},t)-T_{SUB}(z=d_M+d_{SL},t)]}{R_{th,SL-SUB}} \quad (4)$$

where d_{SL} is the thickness of the superlattice layer, $T_{SL}(z = d_M + d_{SL}, t)$ is the temperature at the bottom surface of the superlattice, $T_{SUB}(z = d_M + d_{SL}, t)$ is the temperature at the top surface of the substrate, and $R_{th,SL-SUB}$ is the thermal boundary

resistance between the superlattice and the substrate. Finally, the heat flow in the substrate is given by:

$$C_{SUB}\frac{\partial T_{SUB}(z,t)}{\partial t} = \kappa_{SUB}\frac{\partial^2 T_{SUB}(z,t)}{\partial z^2} \quad (5)$$

where C_{SUB} is the heat capacity of the substrate, $T_{SUB}(z,t)$ is the temperature profile in the substrate at time t and distance z from the metal surface, and κ_{SUB} is the thermal conductivity of the substrate. The substrate is treated as a semi-infinite solid because it is much thicker than the transducer and superlattice.

The bulk heat capacity values are used for the transducer layer and the substrate. A weighted average of the bulk heat capacity values of the constituent materials is used for the superlattice. The bulk thermal conductivity is used for the substrate, a reduced thermal conductivity (determined using the Wiedemann-Franz law [32], FDTR [33], or an analytic model [34]) is used for the transducer layer, and the thermal conductivity of the superlattice is a free parameter.

Since our experimental time delay is not a large fraction of the time between pulses [1], particularly for the amplifier system, we do not include the effects of pulse accumulation in our simulation. If this assumption is incorrect, then our analysis would overestimate the thermal conductivity of the sample. This is because when pulses accumulate, the actual change in temperature of the transducer layer is larger than the change in temperature due to a single pump pulse. If the change in temperature is larger over the same change in time, then the heat flux is larger. So, when the cooling curve is analyzed without considering the effects of pulse accumulation, it looks like the material is dissipating more heat than it actually is, which results in a larger thermal conductivity. However, as stated previously, pulse accumulation should not be an issue in our analysis because of the time delays used are small compared to the time between pulses.

The applicability of Fourier's Law to describe the heat flow in nanoscale structures has been questioned [35] because the macroscopic definition of local temperature in non-equilibrium heat flow may not be valid at the nanoscale level. However, we can still extract an effective thermal conductivity from our TDTR data using Fourier's Law.

Chapter 4: Results and Discussion

This chapter includes details about the samples used for testing, the experimental data, and the thermal conductivity and interface resistance fitting results. The sensitivity of the model to various material properties will also be discussed.

4.1: SAMPLES

Several GaAs/AlAs superlattice samples are tested in this thesis. Because GaAs/AlAs superlattices have been studied for decades [4, 36, 37, 38], there are widely accepted thermal conductivity values to which we can compare our results from our two experimental apparatus. The samples were grown by molecular beam epitaxy (MBE). The SLs were grown on a 500 nm AlAs etch release layer which is on top of a 150 nm GaAs buffer layer which is on top of a GaAs substrate (See Figure 3.).

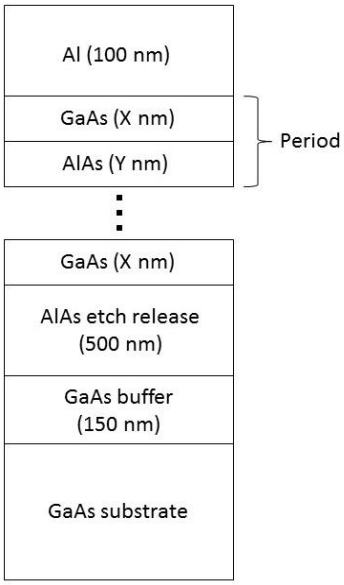

Figure 3: Schematic of GaAs/AlAs superlattice samples with Al transducer layer, AlAs etch release layer, GaAs buffer, and GaAs substrate.

The samples will be referred to by the layer thicknesses of GaAs and AlAs in one period. For example, 1x1 refers to the sample with a superlattice period made of 1 nm of GaAs and 1 nm of AlAs. The dimensions of each SL sample are listed in Table 1. All of the samples except 40x1, have a superlattice period with a 1:1 ratio of GaAs to AlAs. The samples all have the same number of periods, 30, except one of the 8x8 SLs which has 219 periods. Comparing the two 8x8 samples with a different number of periods will give some insight into whether the thermal conductivity depends only on superlattice period or if there is some dependence on the overall thickness of the SL. On top of each sample is a 100 nm Al transducer layer. Aluminum was chosen as the transducer metal because it has the best responsivity at the probe wavelength of 800 nm [39]. To ensure the Al film is thick enough that the light does not penetrate the sample and thin enough that the temperature gradient in the Al is minimized, Capinski and Maris et al. [4] determined that the best thickness for Al is between 80 nm and 120 nm. The Al layer was deposited on all the samples at the same time so the thickness is consistent across all samples.

Table 1: Superlattice Sample Dimensions

Sample	**GaAs (X nm)**	**AlAs (Y nm)**	**# of periods**	**Total SL thickness (nm)**
1x1	1	1	30	61
2x2	2	2	30	122
3x3	3	3	30	183
6x6	6	6	30	366
8x8	8	8	30	488
8x8 219p	8	8	219	3512
40x1	40	1	30	1270

4.2: EXPERIMENTAL DATA AND FITTING

The following section includes the experimental data and fitting results for the TDTR data measured with the oscillator apparatus and the amplifier apparatus. The sensitivity of the model to various parameters is also included.

The experimental time delay can be limited by the length and stability of the mechanical delay stage, but a minimum time delay is needed to resolve the thermal boundary resistance between the transducer and the superlattice. Stevens et al. [29] developed an interface time constant $\tau_i = C_M d_M R_{th,M-SL}$ where the time delay must be larger than the interface time constant to determine the thermal boundary resistance. However, calculating the time constant requires accurately knowing the range of the unknown resistance. Huxtable et al. [25] recommends a time delay between 1 ns and 4 ns. Costescu et al. [24] has shown that the time delay required decreases with decreasing thermal boundary resistance, which is the same trend as the interface time constant calculation. Our time delay choice was based on the stability of our delay stage and the overall data collection time. We used a time delay of 2.4 ns for the oscillator system and 1.5 ns for the amplifier system.

For all the samples except the 1x1 sample, the thermal boundary resistance between the SL and the GaAs substrate does not have any effect on the cooling curve, so the only fitting parameters are the thermal conductivity of the SL and the thermal boundary resistance between the Al and the SL. Whether the interface between the SL and substrate will be important to the cooling curve can be determined by calculating the diffusion length within the superlattice. Using an estimated thermal conductivity of 7 W/(m*K) to calculate the thermal diffusivity of the 1x1 sample, the diffusion length at a 2.5 ns time delay is 99 nm, which is larger than the thickness of the superlattice. To determine the thermal conductivity of the 1x1 SL sample, the SL was treated as a thermal

resistance between the Al layer and the 500 nm AlAs layer. So, in the analysis, the first layer is 100 nm of Al, the second layer is 500 nm of AlAs, and the substrate is GaAs. The thermal resistance between the Al and AlAs, given by:

$$R_{th,Al-AlAs} = R_{th,Al-SL} + {}^{d_{SL}}/_{\kappa_{SL}} + R_{th,SL-AlAs} \quad (6)$$

contains the interface resistance between the Al and SL, the thermal resistance caused by the thickness of the SL and its thermal conductivity (d_{SL}/κ_{SL}), and the interface resistance between the SL and AlAs all added together in series.

During the first 100 ps or so, the electrons and phonons in the Al are redistributing the heat within the film through non-equilibrium processes. To better describe this short period of time, a more complex model, such as the two-step model [40], can be utilized, but it does not change the cooling curve significantly beyond that thermalization time. Because our analysis does not account for the initial non-equilibrium heating, the experimental data is normalized at 160 ps for comparison to the thermal model.

4.2.1: Oscillator results

The thermal resistance fitting for the oscillator TDTR data for the 1x1 sample is shown in Figure 4(a). The superlattice thermal conductivity and thermal boundary resistance fittings for the TDTR measurements collected using the oscillator apparatus are shown in Figures 4(b)-(f) for the 2x2, 3x3, 6x6, 8x8, and 40x1 samples, respectively. The values are summarized in Table 2. A fitting for the 8x8 sample with 219 periods is not included because there was a significant error in the data which caused the ΔR/R value to fall below zero. The error may have been caused by the formation of an oxide layer on the Al or melting of the sample.

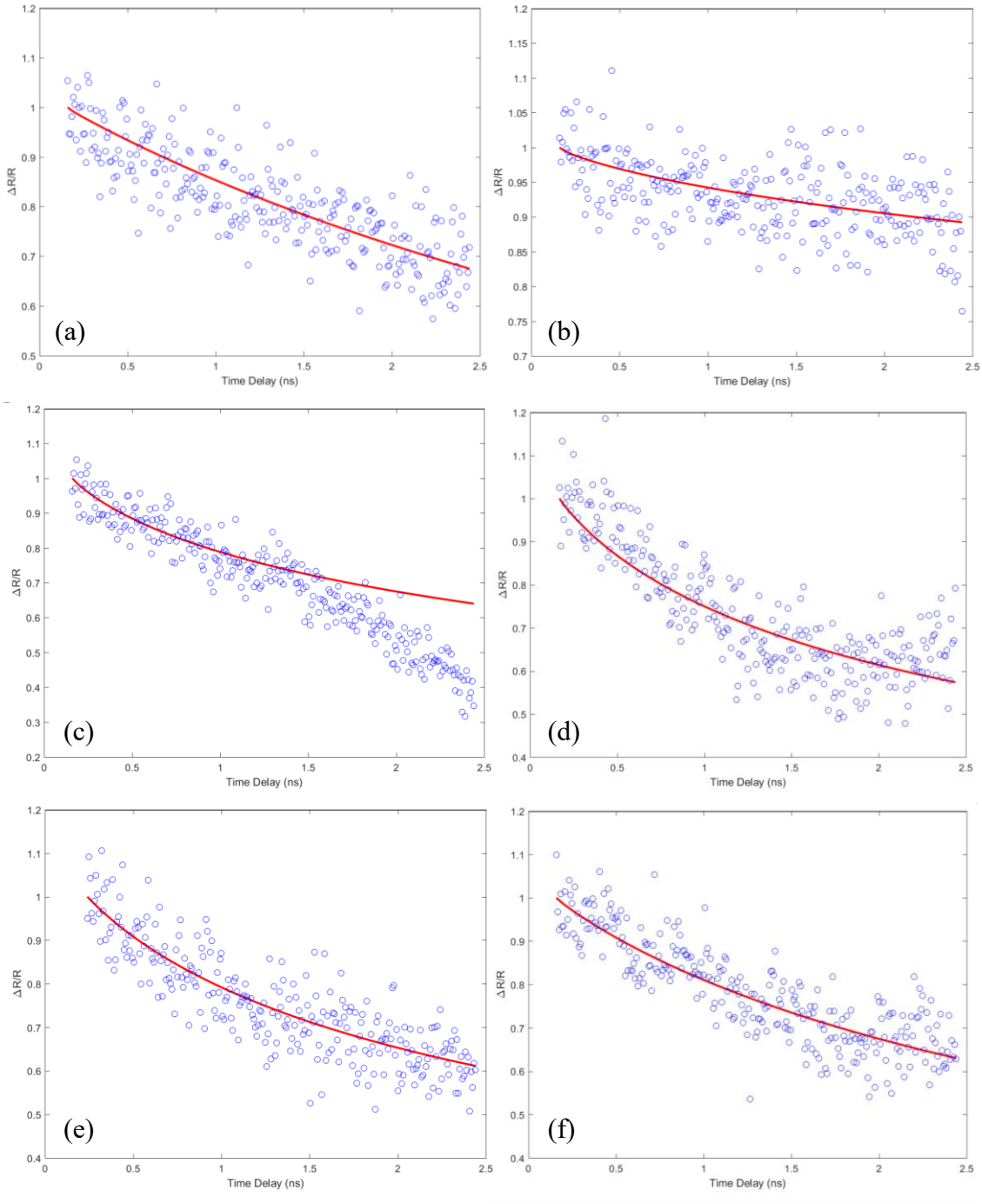

Figure 4: Fitting results of the oscillator apparatus TDTR data for the (a) 1x1, (b) 2x2, (c) 3x3, (d) 6x6, (e) 8x8, and (f) 40x1 GaAs/AlAs samples. The blue circles represent the experimental data, and the red line represents the fitting.

For the 3x3 and 6x6 samples, the entire data sets are displayed, but they were only fitted to 1.4 ns and 1.8 ns, respectively. The data for those two samples showed a clear change in slope after that time delay which may have been due to instability of the mechanical delay stage or slight accidental movement of the table. The data for all the other samples were fitted for the whole delay time.

The thermal conductivity of the 1x1 was calculated using estimated thermal boundary resistances. The thermal boundary resistance for the Al-SL interface was chosen based on the amplifier results. The thermal boundary resistance for the SL-AlAs interface was chosen to be smaller than the Al-SL resistance because of the small lattice mismatch between GaAs and AlAs. Looking at Table 2, there is not a clear trend between the thermal conductivity and the superlattice period thickness. A more thorough discussion of the results and how they compare to the amplifier results and literature values is included in section 4.3.

Table 2: Thermal Conductivity and Thermal Boundary Resistance Fitted Values for Oscillator Apparatus TDTR Data

Sample	**κ [W/(m*K)]**	**R_{th}(m^2K/W)**
1x1	17 (R_{total}=9.5x10^{-9})	$R_{th,Al-SL}$ = 4x10^{-9}
		$R_{th,SL-AlAs}$ = 2x10^{-9}
2x2	0.56	10x10^{-9}
3x3	11	2.3x10^{-9}
6x6	21	2.3x10^{-9}
8x8	19.6	2.7x10^{-9}
40x1	27	5.4x10^{-9}

4.2.2: Amplifier results

The interface resistance fitting for the amplifier TDTR data for the 1x1 sample is shown in Figure 5(a). The superlattice thermal conductivity and thermal boundary resistance fittings for the TDTR measurements collected using the amplifier apparatus are shown in Figures 5(b)-(g) for the 2x2, 3x3, 6x6, 8x8, 8x8 219p and 40x1 samples, respectively. The values are summarized in Table 3.

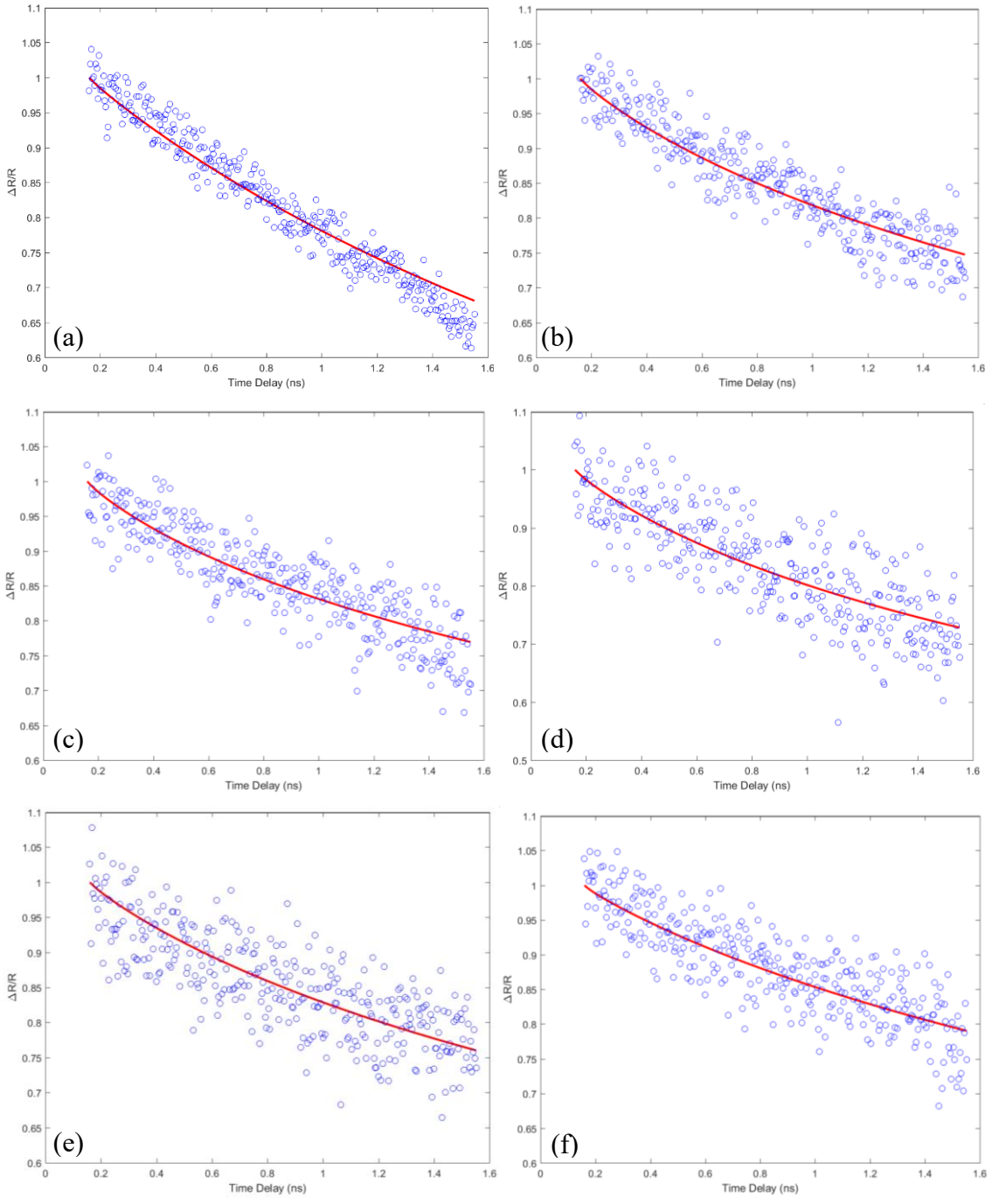

Figure 5: Fitting results of the amplifier apparatus TDTR data for the (a) 1x1, (b) 2x2, (c) 3x3, (d) 6x6, (e) 8x8, (f) 8x8 219p and (g) 40x1 GaAs/AlAs samples. The blue circles represent the experimental data, and the red line represents the fitting.

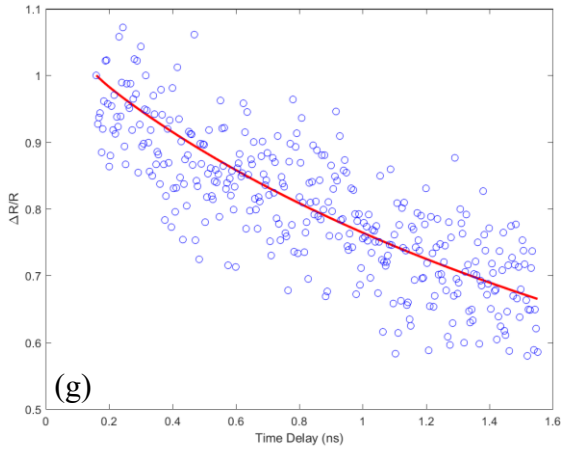

Figure 5, continued

The model seems to deviate from the experimental data for the 1x1 samples at the beginning and the end of the time delay. The model follows the amplifier apparatus experimental data well for the six other samples over the entire delay time. The fitted thermal resistance value for the 1x1 sample is smaller than the sum of the two boundary resistances, which would result in a negative thermal conductivity. This is not a reasonable result, so the sample may be too thin for our apparatus to accurately measure. The thermal conductivities and resistances for the 2x2, 3x3, 6x6, 8x8, and 8x8 219p samples are all very similar. A more thorough discussion of the results and how they compare to the oscillator results and literature values is included in the next section.

Table 3: Thermal Conductivity and Thermal Boundary Fitted Values for Amplifier Apparatus TDTR Data

Sample	**κ [W/(m*K)]**	**R_{th}(m^2K/W)**
1x1	(R_{total}=5.4x10^{-9})	$R_{th,Al-SL}$ = 4x10^{-9}
		$R_{th,SL-AlAs}$ = 2x10^{-9}
2x2	11.8	4.3x10^{-9}
3x3	7.5	3.7x10^{-9}
6x6	13	3.5x10^{-9}
8x8	11	4.8x10^{-9}
8x8 219p	10	6.5x10^{-9}
40x1	56	4.3x10^{-9}

4.3: DISCUSSION

Figure 6 compares the SL thermal conductivity values for the 1x1 (oscillator only), 2x2, 3x3, 6x6, 8x8, and 8x8 219p (amplifier only) samples to the values obtained by Capinski and Maris et al [4]. Since the ratio of GaAs to AlAs is not 1:1 in the 40x1 sample, it is not included in Figure 6. However, because the 40x1 sample is primarily GaAs, it is expected that the SL thermal conductivity is equivalent to the thermal conductivity of bulk GaAs, κ_{GaAs}=55 W/(m*K).

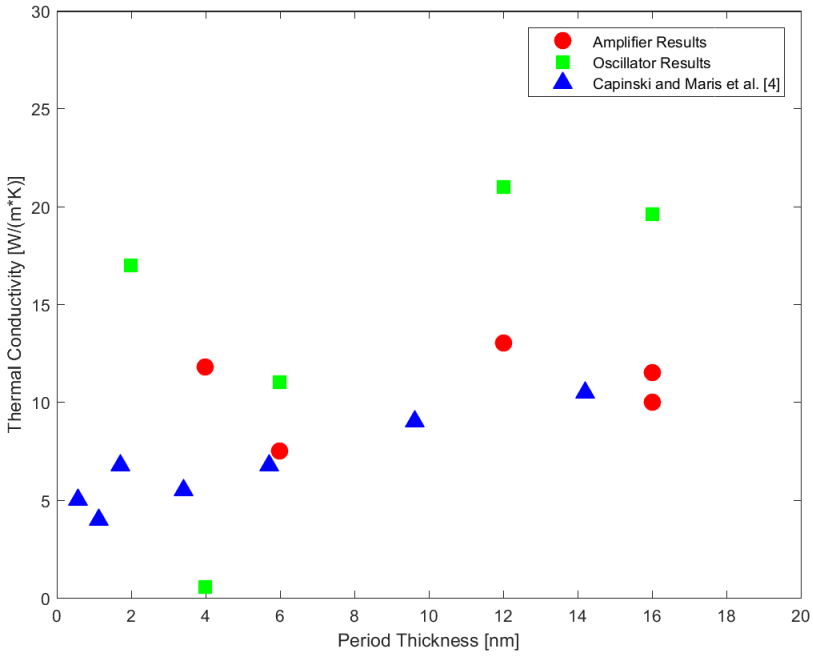

Figure 6: Superlattice thermal conductivity as a function of superlattice period thickness for GaAs/AlAs. Amplifier and oscillator results from this work are represented by the circles and squares, respectively. Results from Capinski and Maris et al. are represented by triangles.

The oscillator data largely overestimated the thermal conductivity for the 1x1, 6x6, and 8x8 samples, and slightly overestimated the 3x3 thermal conductivity. Since we did not account for pulse accumulation in our analysis, we would expect the model to give larger thermal conductivities for the oscillator system, so this may be the source of the error. However, the thermal conductivities for the 2x2 and 40x1 were severely underestimated by the oscillator data, which cannot be explained by pulse accumulation. We only took our measurements at one spot on each sample, so is it highly possible that human error impacted the measurements. The optics in the oscillator system are more complex than those in the amplifier system and require careful tuning to get accurate results. There were clear changes in signal for the 3x3 and 6x6 samples beyond 1.4 ns

and 1.8 ns, respectively, and we did not even get measurements that could be fitted from the 8x8 219p sample. Other than the 1x1 sample, we did not have those errors when using the amplifier system, even though we only took measurements at one spot on each sample in that setup as well.

The thermal conductivity results from the amplifier are much closer to the literature values. The thermal conductivity of the 40x1 sample perfectly aligns with the thermal conductivity of bulk GaAs, as expected. The results for 3x3, 6x6, 8x8, and 8x8 219p are well within the range of the thermal conductivities reported by Capinski and Maris et al. [4]. We could not get a thermal conductivity value from the 1x1 measurements, and the value for the 2x2 sample is much larger than the value obtained in literature.

The thermal boundary resistance between the Al and SL should be about the same for all samples because the Al deposition method was the same. However, this is not the case for the oscillator results. There is large difference between the smallest resistance, 2.3×10^{-9} m^2K/W for 3x3 and 6x6, and the largest resistance, 10×10^{-9} m^2K/W for 2x2. On the other hand, the resistances from the amplifier results are fairly consistent across the samples. This along with the consistency of the thermal conductivity results, leads us to conclude that the amplifier apparatus gives more reliable TDTR measurements than the oscillator apparatus.

The measurements from neither the oscillator setup nor the amplifier setup gave reasonable thermal conductivity values for the 1x1 sample. It is possible that this sample is too thin for our apparatus to accurately measure. The thinnest GaAs/AlAs sample measured by Capinski and Maris et al. [4] was 212 nm. To get an accurate measurement of a 1x1 SL, we may need to use a sample with more superlattice periods so the overall thickness of the superlattice is larger.

4.4: SENSITIVITY STUDY

The sensitivity of the model to certain parameters, such as the thermal boundary resistance and SL thermal conductivity, can be calculated with the method used by Costescu et al [24]:

$$|S_x| = \left|\frac{\partial(\ln \mathrm{T(t)})}{\partial(\ln x)}\right| \tag{7}$$

where S_x is the sensitivity of the temperature $\mathrm{T(t)}$ to the parameter x. Since our analysis is solved using the finite difference method, Equation 7 is estimated as:

$$|S_x| = \left|\frac{\ln(T_{1.1x}(t)) - \ln(T_{0.9x}(t))}{\ln(1.1x) - \ln(0.9x)}\right| \tag{8}$$

where $T_{1.1x}(t)$ and $T_{0.9x}(t)$ are the temperatures at time t when parameter x is 110% and 90% of its fitted value, respectively. The sensitivity can be used to determine the time delay needed to resolve certain parameters; it is also used to calculate uncertainty [15].

The sensitivity is presented for the thinnest sample, 1x1, a moderate sample, 8x8, and the sample with the largest thermal conductivity, 40x1. The sensitivity is based on the thermal conductivity and thermal boundary resistance values from the amplifier apparatus measurements for 8x8 and 40x1, rather than the results from the oscillator setup, because they were more consistently aligned with the literature values. For the 1x1 sample, the sensitivity for all parameters is plotted twice: one plot is based on the thermal interface resistance determined from the oscillator results and the second plot is based on the expected thermal interface resistance using the literature value for thermal conductivity, $R_{th}{\sim}15x10^{-9}$ $\mathrm{m^2K/W}$. The sensitivity of the temperature to the thermal conductivity of the Al layer, the thermal resistance between the Al and AlAs, the thermal conductivity of the AlAs, the thickness of the Al layer, and the thickness of the AlAs layer is shown in Figures 7(a) and 7(b) for the 1x1 sample using the experimental resistance and the expected resistance, respectively. The sensitivity of the temperature to the thermal conductivity of the Al layer, the thermal resistance between the Al and SL,

the thermal conductivity of the SL, the thickness of the Al layer, and the thickness of the SL is shown in Figures 7(c) and 7(d) for the 8x8 and 40x1 samples, respectively.

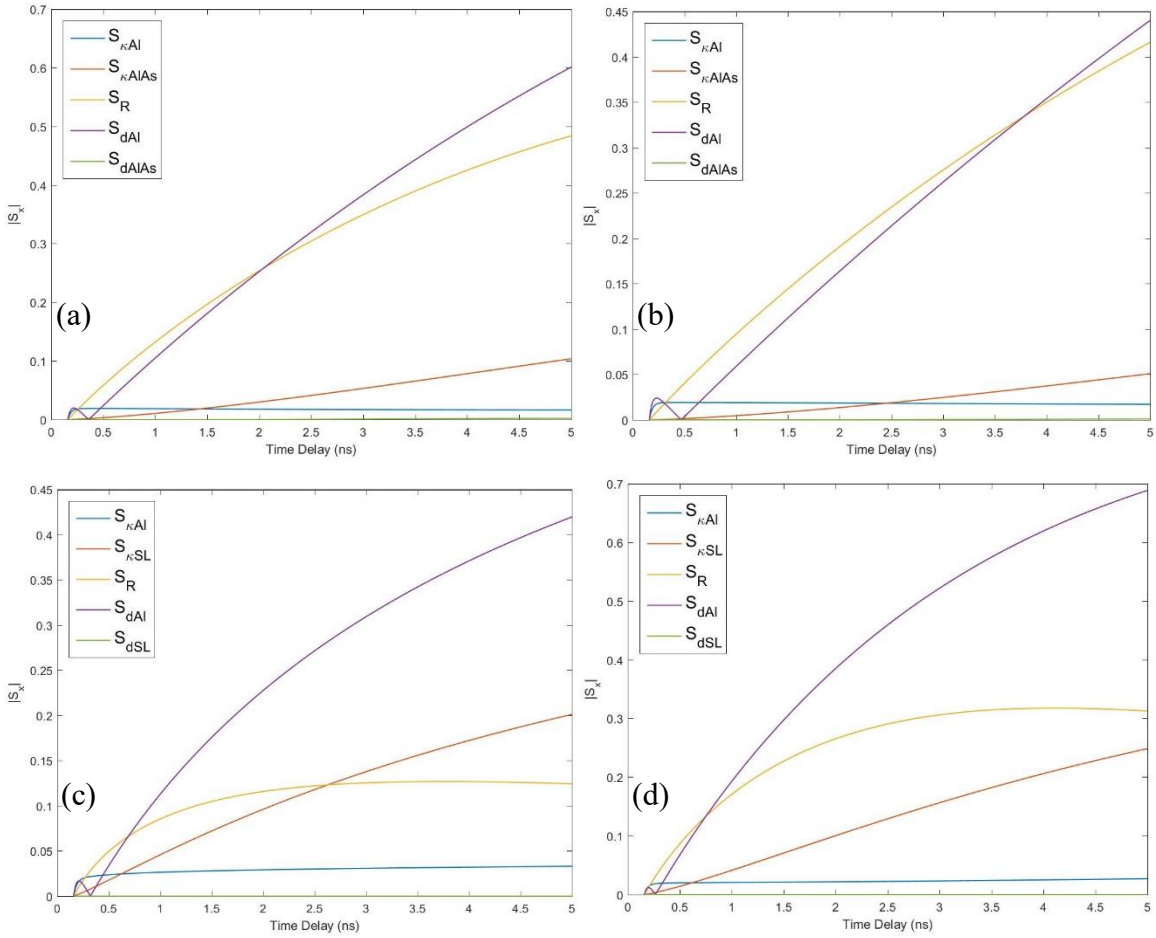

Figure 7: Sensitivity analysis of the model to sample parameters for (a) the 1x1 sample using the fitted total interface resistance value for the oscillator results, (b) the 1x1 sample using the expected total interface resistance, (c) the 8x8 sample, and (d) the 40x1 sample both using the fitted values from the amplifier results.

In both cases, the results for the 1x1 sample are insensitive to the thermal conductivity of the AlAs layer, but highly sensitive to the thermal resistance. Also, the results are more sensitive to the thermal resistance and less sensitive to the AlAs thermal

conductivity for the plot using the expected total interface resistance value, which is larger than the value from the oscillator measurements. Since the sensitivity to the interface resistance is large, a small change in the resistance creates a large change in the model results, so we should be able to accurately determine the thermal resistance with low uncertainty.

For the 8x8 and 40x1 samples, the sensitivity to the thermal boundary resistance saturates at about 2.5 ns, but sensitivity to thermal conductivity continues to increase. Thus, a time delay of at least 2.5 ns should be used to determine the resistance, which is right in the middle of the time delay suggested by Huxtable et al. [25]. Although 2.5 ns should be sufficient to determine the thermal conductivity, increasing the time delay could further reduce the uncertainty of the thermal conductivity results, so if the mechanical delay stage is long enough and stable enough, a longer delay time is recommended.

Like the 1x1 sample, the 40x1 sample is more sensitive to the thermal resistance than the thermal conductivity of the second layer (AlAs in the 1x1 sample and the SL in the 40x1 sample) over the 5 ns time delay. Since the 8x8 and 40x1 samples have similar thermal resistance values, but the 8x8 sample does not show this trend, the higher sensitivity to the resistance is likely due to the high thermal conductivity of the second layer. This is reasonable because a material with a high thermal conductivity will cause a smaller change in temperature compared to a low thermal conductivity material for the same heat flux. This means the cooling is dominated by the thermal boundary resistance when the thermal conductivity of the second layer is large.

The results for all three samples (1x1, 8x8, and 40x1) are generally most sensitive to the thickness of the Al layer, which aligns with the uncertainty analysis completed by Yang et al. [15] that shows the largest source of error in TDTR measurements comes

from the accuracy of the transducer thickness measurement. The thermal conductivity of 100 nm Al is approximately 110 W/(m*K) in some calculations [4, 34] and 200 W/(m*K) in others [32, 33], but the sensitivity for the representative samples presented shows that the Al thermal conductivity has little impact on the cooling curve beyond the first 160 ps. Using either value in the analysis should result in the same fitted thermal conductivity and thermal boundary resistance for the sample.

The results are also insensitive to the thickness of the SL for the 8x8 and 40x1 samples and the thickness of the AlAs for the 1x1 sample. This is because, even at 5 ns, the diffusion length for these samples is shorter than the thickness of the second layer (SL or AlAs). However, at 5 ns the diffusion length is longer than the SL thickness for the 2x2 sample, so the 500 nm AlAs may need to be included in the analysis. To avoid the interaction with the AlAs layer, a time delay of less than approximately 3 ns should be used, which is still long enough the resolve the resistance and thermal conductivity.

Chapter 5: Future Work and Conclusion

5.1: Future Work

First and most importantly, the experimental tests, especially for the oscillator apparatus, need to be repeated at several points on each sample to check if the data is repeatable. Based on the sensitivity analysis, the TDTR measurements should also be repeated with longer delay time to better resolve the thermal conductivity and thermal boundary resistance.

Luckyanova et al. [41] experimentally showed that the thermal conductivity of GaAs/AlAs SLs with periods of 12 nm GaAs and 12nm AlAs increases with increasing number of periods from one to nine periods. The amplifier results for the 8x8 SL with 30 periods and the 8x8 SL with 219 periods show that the two samples have essentially the same thermal conductivity. It would be interesting to investigate whether the thermal conductivity value saturates at a certain number of periods and if that number of periods is the same regardless of period thickness.

It may also be useful to measure the thermal conductivity of GaAs/AlAs SLs with the same period thickness, but vary the ratio of GaAs and AlAs within the period from sample to sample. In a study of InGaAs/InAlAs superlattices, Sood et al. [42] showed that the thermal conductivity of the SL increases linearly with increasing the proportion of InGaAs in the period and decreases linearly with increasing the proportion of InAlAs. Bulk InGaAs has a larger thermal conductivity than bulk InAlAs, so intuitively it makes sense than the thermal conductivity of the SL would increase when the amount of the material with the larger thermal conductivity increases. We varied the ratio of GaAs and AlAs in one sample, but a more systematic approach should be taken to draw meaningful conclusions.

Sood et al. [42] also showed that the thermal conductivity of two SL samples with the same number of periods and a 1:1 ratio of constituent materials had the same thermal conductivity. They attributed this behavior to the highly specular scattering at the period interfaces due to the lattice match between InGaAs and InAlAs. GaAs and AlAs have a very small lattice mismatch [5] so it may be possibly to see this same behavior in GaAs/AlAs superlattices. All but two of our samples had the same number of periods and a 1:1 ratio of materials, and the amplifier data gave very similar thermal conductivities for all of those samples, except the 1x1 sample. However, the GaAs/AlAs SL thermal conductivity values measured by Capinski and Maris et al. [4] generally increased with increasing superlattice period thickness, but neither the number of periods nor the overall SL thickness was held constant across their samples, so it is difficult to determine if other factors influenced the trend.

To aid in concluding whether the thermal conductivities of our GaAs/AlAs SL samples with the same number of periods and 1:1 thickness ratio of materials are the same, a thorough calculation of uncertainty should be completed. Using the sensitivity of the model and the accuracies in the measurement, the uncertainties of the thermal conductivity and thermal boundary resistance can be determined. The uncertainty and several repeatable measurements would allow us to be more confident about the results we obtained.

5.2: CONCLUSION

In this thesis, we took time-domain thermoreflectance measurements of seven GaAs/AlAs superlattice sample using two different experimental setups. The first setup utilized a Ti:sapphire laser to produce pulses at a 76 MHz repetition rate, and the second setup used an amplifier to produce pulses at a 5 kHz repetition rate. The amplifier apparatus also used a two-color pump-probe arrangement to simplify the optics involved with detecting the probe signal. We used a one-dimensional conduction model solved using the finite difference method to analyze the heat flow through the samples. Using this analysis, we determined the thermal conductivities of the superlattices and the thermal boundary resistances between the Al transducer layer and the superlattices. We also completed a sensitivity analysis after testing the samples, but it would be good practice to do the sensitivity analysis with estimated values before testing to determine the appropriate delay time for each sample.

Although the tests should be repeated for all samples with both experimental setups to ensure the results we obtained can be replicated, the thermal conductivity results from the amplifier system more consistently aligned with the literature values. The thermal boundary resistance values measured using the amplifier setup were also more consistent from sample to sample, which is expected considering the deposition of the Al was completed simultaneously for all samples. The 3x3 sample is the only sample to have reasonable thermal conductivity results from both experimental setups. The oscillator measurements overestimated the thermal conductivity of four of the samples, most likely because we did not include pulse accumulation in our analysis. Neither apparatus gave reasonable results for the 1x1 sample, so the 61 nm SL may be too thin for an accurate thermal conductivity measurement with our current TDTR technique.

The sensitivity analysis shows that the sensitivity to the thermal boundary resistance saturates after about 2.5 ns, so the resistance measurement will not benefit from a longer delay time. However, the sensitivity to the SL thermal conductivity continues to increase over the time delay, so increasing the delay time may reduce the uncertainty in the thermal conductivity measurement as long as the delay stage is stable and the pump and probe stay well aligned. When choosing the time delay, the diffusion length within the SL should also be calculated to determine if there will be any substrate interaction. If the diffusion length at the maximum time delay is longer than the thickness of the SL, the time delay should be decreased or the interaction with the substrate has to be included in the analysis. However, decreasing the time delay may also decrease the sensitivity to the resistance and thermal conductivity, so for our apparatus the minimum time delay is 2.5 ns which makes the minimum superlattice thickness about 120 nm with a diffusivity of $D=6x10^{-5}$ m^2/s.

The amplified laser requires more equipment and is more expensive than the oscillator, but we were able to get more consistent thermal conductivity and thermal boundary resistance results for most of the GaAs/AlAs SL samples. Additionally, the sensitivity analysis shows that the thermal conductivity measurement would benefit from a longer time delay, but as the time delay becomes a larger fraction of the time between pulses, pulse accumulation may introduce errors into the oscillator results. To continue using the simple one-dimensional heat flow analysis described in the work and a longer time delay, the amplifier system is recommended to minimize pulse accumulation and achieve reliable results for superlattice samples thicker than approximately 120 nm.

References

[1] D. G. Cahill, W. K. Ford, K. E. Goodson, G. D. Mahan, A. Majumdar, H. J. Maris, R. Merlin and R. S. Phillpot, "Nanoscale thermal transport," *Journal of Applied Physics,* vol. 93, pp. 793-818, 2003.

[2] M. S. Dresselhaus, G. Dresselhaus, X. Sun, Z. Zhang, S. B. Cronin, T. Koga, J. Y. Ying and G. Chen, "The promise of low-dimensional thermoelectric materials," *Microscale Thermophysical Engineering,* vol. 3, pp. 89-100, 1999.

[3] W. Kim, J. Zide, A. Gossard, D. Klenov, S. Stemmer, A. Shakouri and A. Majumdar, "Thermal conductivity reduction and thermoelectric figure of merit increase," *Physical Review Letters,* vol. 96, p. 045901, 2006.

[4] W. S. Capinski, H. J. Maris, T. Ruf, M. Cardona, K. Ploog and D. S. Katzer, "Thermal-conductivity measurements of GaAs/AlAs superlattices using a picosecond optical pump-and-probe technique," *Physical Review B,* vol. 59, pp. 8105-8113, 1999.

[5] S. P. Hepplestone and G. P. Srivastava, "Lattice dynamics and thermal properties of phononic semiconductors," *Physical Review B,* vol. 84, p. 115326, 2011.

[6] S.-.. Lee, D. G. Cahill and R. Venkatasubramanian, "Thermal conductivity of Si–Ge superlattices," *Applied Physics Letters,* vol. 70, pp. 2957-2959, 1997.

[7] T. Borca-Tasciuc, W. Liu, J. Liu, T. Zeng, D. W. Song, C. D. Moore, G. Chen, K. L. Wang, M. S. Goorsky, T. Radetic, R. Gronsky, T. Koga and M. S. Dresselhaus, "Thermal conductivity of symmetrically strained Si/Ge superlattices," *Superlattices and Microstructures,* vol. 28, pp. 199-206, 2000.

[8] A. J. Schmidt, R. Cheaito and M. Chiesa, "A frequency-domain thermoreflectance method for the characterization of thermal," *Review of Scientific Instruments,* vol. 80, p. 094901, 2009.

[9] Y. Ezzahri, S. Dilhaire, S. Grauby, J. M. Rampnoux, W. Claeys, Y. Zhang, G. Zeng and A. Shakouri, "Study of thermomechanical properties of Si/SiGe superlattices using femtosecond transient thermoreflectance technique," *Applied Physics Letters,* vol. 87, p. 103506, 2005.

[10] M. N. Touzelbaev, P. Zhou, R. Venkatasubramanian and K. E. Goodson, "Thermal characterization of Bi_2Te_3/Sb_2Te_3 superlattices," *Journal of Applied Physics,* vol. 90, pp. 763-767, 2001.

[11] D. G. Cahill and R. O. Pohl, "Thermal conductivity of amorphous solids above the plateau," *Physical Review B,* vol. 35, pp. 4067-4073, 1987.

[12] Y. K. Koh, S. L. Singer, W. Kim, J. M. O. Zide, D. G. Cahill, A. Majumdar and A. C. Gossard, "Comparison of the 3ω method and time-domain thermoreflectance for measurements of cross-plane thermal conductivity of epitaxial semiconductors," *Journal of Applied Physics,* vol. 105, p. 054303, 2009.

[13] D. G. Cahill, K. Goodson and A. Majumdar, "Thermometry and thermal transport in micro/nanoscale solid-state devices and structures," *Journal of Heat Transfer,* vol. 124, pp. 223-241, 2002.

[14] J. Zhu, D. Tang, W. Wang, J. Liu, K. W. Holub and R. Yang, "Ultrafast thermoreflectance techniques for measuring thermal conductivity and interface thermal conductance of thin films," *Journal of Applied Physics,* vol. 108, p. 094315, 2010.

[15] J. Yang, E. Ziade and A. J. Schmidt, "Uncertainty analysis of thermoreflectance measurements," *Review of Scientific Instruments,* vol. 87, p. 014901, 2016.

[16] C. A. Paddock and G. L. Eesley, "Transient thermoreflectance from thin metal films," *Journal of Applied Physics,* vol. 60, pp. 285-290, 1986.

[17] J. Cho, Z. Li, E. Bozorg-Grayeli, T. Kodama, D. Francis, F. Ejeckam, F. Faili, M. Asheghi and K. E. Goodson, "Thermal characterization of GaN-on-diamond substrates for HEMT applications," in *13th InterSociety Conference on Thermal and Thermomechanical Phenomena in Electronic Systems*, 2012.

[18] A. Soni, V. M. Sundaram and S.-B. Wen, "A methodology for nanosecond (or better) time resolved thermoreflectance imaging with coherence control of laser pulses," *Applied Physics Letters,* vol. 102, p. 203112, 2013.

[19] C. A. Paddock and G. L. Eesley, "Transient thermoreflectance from metal films," *Optics Letters,* vol. 11, pp. 273-275, 1986.

[20] W. S. Capinski and H. J. Maris, "Thermal conductivity of GaAs/AlAs superlattices,"

Physica B: Condensed Matter, Vols. 219-220, pp. 699-701, 1996.

[21] W. S. Capinski and H. J. Maris, "Improved apparatus for picosecond pump-and-probe optical measurements," *Review of Scientific Instruments,* vol. 67, pp. 2720-2726, 1996.

[22] A. J. Schmidt, X. Chen and G. Chen, "Pulse accumulation, radial heat conduction, and anisotropic thermal conductivity in pump-probe transient thermoreflectance," *Review of Scientific Instruments,* vol. 79, p. 114902, 2008.

[23] D. G. Cahill, "Analysis of heat flow in layered structures for time-domain thermoreflectance," *Review of Scientific Instruments,* vol. 75, pp. 5119-5122, 2004.

[24] R. M. Costescu, M. A. Wall and D. G. Cahill, "Thermal conductance of epitaxial interfaces," *Physical Review B,* vol. 57, p. 054302, 2003.

[25] S. Huxtable, D. G. Cahill, V. Fauconnier, J. O. White and J.-C. Zhao, "Thermal conductivity imaging at micrometre-scale resolution for combinatorial studies of materials," *Nature Materials,* vol. 3, pp. 298-301, 2004.

[26] M. Highland, B. C. Gundrum, Y. K. Koh, R. S. Averback, D. G. Cahill, V. C. Elarde, J. J. Coleman, D. A. Walko and E. C. Landahl, "Ballistic-phonon heat conduction at the nanoscale as revealed by time-resolved x-ray diffraction," *Physical Review B,* vol. 76, p. 075337, 2007.

[27] Z. Ge, D. G. Cahill and P. V. Braun, "Thermal conductance of hydrophilic and hydrophobic interfaces," *Physical Review Letters,* vol. 96, p. 186101, 2006.

[28] H.-K. Lyeo and D. G. Cahill, "Thermal conductance of interfaces between highly dissimilar materials," *Physical Review B,* vol. 73, p. 144301, 2006.

[29] R. J. Stevens, A. N. Smith and P. M. Norris, "Measurement of thermal boundary conductance of a series of metal-dielectric interfaces by the transient thermoreflectance technique," *Journal of Heat Transfer,* vol. 127, p. 315, 2005.

[30] K. C. Collins, A. A. Maznev, J. Cuffe, K. A. Nelson and G. Chen, "Examining thermal transport through a frequency-domain representation of time-domain thermoreflectance data," *Review of Scientific Instruments,* vol. 85, p. 124903, 2014.

[31] P. M. Norris, A. P. Caffre, R. J. Stevens, J. M. Klopf, J. T. J. McLeskey and A. N. Smith, "Femtosecond pump–probe nondestructive examination of materials (invited)," *Review of Scientific Instruments,* vol. 74, pp. 400-406, 2003.

[32] Y. Wang, J. Y. Park, Y. K. Koh and D. G. Cahill, "Thermoreflectance of metal transducers for time-domain thermoreflectance," *Journal of Applied Physics,* vol. 108, p. 043507, 2010.

[33] A. J. Schmidt, R. Cheaito and M. Chiesa, "Characterization of thin metal films via frequency-domain thermoreflectance," *Journal of Applied Physics,* vol. 107, p. 024908, 2010.

[34] J. M. Lugo and A. I. Olivia, "Thermal properties of metallic films at oom conditions by the heating slope," *Journal of Thermophysics and Heat Transfer,* vol. 30, pp. 452-460, 2016.

[35] R. B. Wilson and D. G. Cahill, "Anisotropic failure of Fourier theory in time-domain thermoreflectance experiments," *Nature Communications,* vol. 5, no. 5075, 2014.

[36] T. Yao, "Thermal properties of AlAs/GaAs superlattices," *Applied Physics Letters,* vol. 51, pp. 1789-1800, 1987.

[37] M. N. Luckyanova, J. A. Johnson, A. A. Maznev, J. Garg, A. Jandl, M. T. Bulsara, E. A. Fitzgerald, K. A. Nelson and G. Chen, "Anisotropy of the thermal conductivity in GaAs/AlAs superlattices," *Nano Letters,* vol. 13, p. 3973, 2013.

[38] X. Y. Yu, G. Chen, A. Verma and J. S. Smith, "Temperature dependence of thermophysical properties of GaAs/AlAs periodic," *Applied Physics Letters,* vol. 67, pp. 3554-3556, 1995.

[39] M. G. Burzo, P. L. Komarov and P. E. Raad, "Optimized thermo-reflectance system for measuring the thermal properties of thin-films and their interfaces," in *Twenty-Second Annual IEEE Semiconductor Thermal Measurement and Management Symposium*, 2006.

[40] T. Q. Qui and C. L. Tien, "Short-pulse laser heating on metals," *International Journal of Heat and Mass Transfer,* vol. 35, pp. 719-726, 1992.

[41] M. N. Luckyanova, J. Garg, K. Esfarjani, A. Jandl, M. T. Bulsara, A. J. Schmidt, A. J. Minnich, S. Chen, M. S. Dresselhaus, Z. Ren, E. A. Fitzgerald and G.

Chen, "Coherent phonon heat conduction in superlattices," *Science,* vol. 338, pp. 936-938, 2012.

[42] A. Sood, J. A. Rowlette, C. G. Caneau, E. Bozorg-Grayeli, M. Asheghi and K. E. Goodson, "Thermal conduction in lattice–matched superlattices of InGaAs/InAlAs," *Applied Physics Letters,* vol. 105, p. 051909, 2014.

[43] H. Wang, Y. Xu, M. Shimono, Y. Tanaka and M. Yamazaki, "Computation of interfacial thermal resistance by phonon diffuse mismatch model," *Material Transactions,* vol. 48, pp. 2349-2352, 2007.